5-2018

Reduction of the Effective Electron Temperature in a Cryogen-Free Dilution Refrigerator via Electronic Filtering and Vibration Dampening

Michael McKinley Yannell
Purdue University

REDUCTION OF THE EFFECTIVE ELECTRON TEMPERATURE IN A CRYOGEN-FREE DILUTION REFRIGERATOR VIA ELECTRONIC FILTERING AND VIBRATION DAMPENING

by

Michael McKinley Yannell

A Thesis

Submitted to the Faculty of Purdue University

In Partial Fulfillment of the Requirements for the degree of

Master of Science in Electrical and Computer Engineering

School of Electrical & Computer Engineering

West Lafayette, Indiana

May 2018

THE PURDUE UNIVERSITY GRADUATE SCHOOL
STATEMENT OF COMMITTEE APPROVAL

Dr. Michael J. Manfra, Chair

Department of Physics and Astronomy

Dr. Gabor Csathy

Department of Physics and Astronomy

Dr. Peide Ye

School of Electrical and Computer Engineering

Approved by:

Dr. Venkataramanan Balakrishnan

Head of the Graduate Program

To Rick, for believing I could achieve more through education.

ACKNOWLEDGMENTS

Firstly I would like to thank my adviser Mike Manfra, for accepting me into your lab as an undergraduate with now research experience and for keeping me around through graduate school. The skills and experiences I have learned during my time in your lab have made me the engineer I am today.

I would also like to thank my mentors Dr. Sumit Mondal and Dr. John Watson for their patience and friendship. To the rest of my colleagues in the Manfra group, especially Geoff Gardner, Saeed Fallahi, Qi Qian, and Jimmy Nakamura for all of your support throughout my graduate experience. Your help has truly been invaluable. And although I say this begrudgingly, Jimmy is almost always right and others would do well to seek out his input more often. And also Charlie Guinn, for being the best undergraduate a person could hope for.

A special thanks to my Purdue family, Kinsey and Ryan Bain, Terry Villarreal, Chris Pulliam, Isaac Marks and Heather Osswald, for allowing me to have a social life while in graduate school and for allowing a non-chemist to hang around. In the future, please don't let Karen win any board games.

Thank you to my 'Ohana in Hawaii, Chicago, Denver, and Washington, D.C. for your support and understanding while I've been so many miles away from all of you. Thank you to my mother, Rosemary K. M. Sword for your endless encouragement. Thank you to my father, John I. Yannell for teaching me the value of hard work.

Thank you to my pets, Dorothy and Klaus for being the best dog-cat combo anyone could expect.

Karen, ko aloha makamae e ipo.

Mahalo nui loa, Na'auaookapueo

TABLE OF CONTENTS

LIST OF TABLES

LIST OF FIGURES

ABSTRACT

Author: Yannell, Michael, M. MSECE
Institution: Purdue University
Degree Received: May 2018
Title: Reduction of the Effective Electron Temperature in a Cryogen-Free Dilution Refrigerator via Electronic Filtering and Vibration Dampening
Committee Chair: Michael J. Manfra

Cryogen-free dilution refrigerators (dry fridges) have become an increasingly popular solution to researchers' cryogenic measurement needs due to their user friendliness and long term use cost savings (^{4}He does not need to be replenished). However, commercially available dry fridges frequently have an effective electron temperatures much warmer than the base temperature of the mixing chamber of the dry fridge. This thesis documents efforts taken to reduce the electron temperature in a dry fridge and the direct probing of the electron temperature via Coulomb blockade thermometry in a 500 nm wide quantum dot.

CHAPTER 1. INTRODUCTION

1.1 Cryogenic Systems

Low temperature (cryogenic) systems are of great interest to academic and industrial researchers. At temperatures near absolute zero, quantum mechanical processes can be observed, such as the quantum Hall effect, Coulomb blockade in quantum dots, electron interferometry, Majorana physics, and super conductivity. Several common cryogenic instruments used to characterize the aforementioned systems are liquid helium refrigerators, ^{3}He refrigerators, and dilution refrigerators.[1] While liquid helium refrigerators reaching temperatures of 4 K and ^{3}He systems reaching temperatures of 300 mK are important, the focus here will be on dilution refrigerators, which commonly reach down to temperatures of 10 mK with temperatures below this being documented.[2-3] They do so by exploiting the phase separation of ^{3}He/^{4}He well below temperatures of 1 K and the preferential evaporation of ^{3}He over ^{4}He, allowing for evaporative cooling of the ^{4}He to temperatures of 10 mK.[1] The details of a dilution refrigerator are explained in section 2.1

1.2 Two Dimensional Electron Systems

A two dimensional electron gas (2DEG) is an electron gas free to move in two dimensions while being confined in the third. 2DEGs are commonly found at the heterojunction interface between two materials, e.g. GaAs/AlGaAs. High quality (high mobility and low impurity) (Al)GaAs heterostructures can be grown using molecular beam epitaxy (MBE), like the samples grown by Professor Manfra in the Birck Nanotechnology Center at Purdue University.[4]

1.2.1 Quantum Hall Effect

The Hall effect is the development of a translational voltage difference across an electrical conductor in a perpendicular applied magnetic field. The quantum Hall effect (QHE) is the quantum mechanical version of this effect which shows quantized value of conductance at values of $\nu e^2/h$, where ν is the Landau level filling factor, e is the electron charge, and h is Planck's constant. Landau levels (LL) are the equally spaced energy levels of a particle in the presence of

an applied magnetic field. The LL filling factor can take integer or fractional values (integer quantum Hall effect and fractional quantum Hall effect). The quantum Hall effect is further discussed in section 2.2.1.

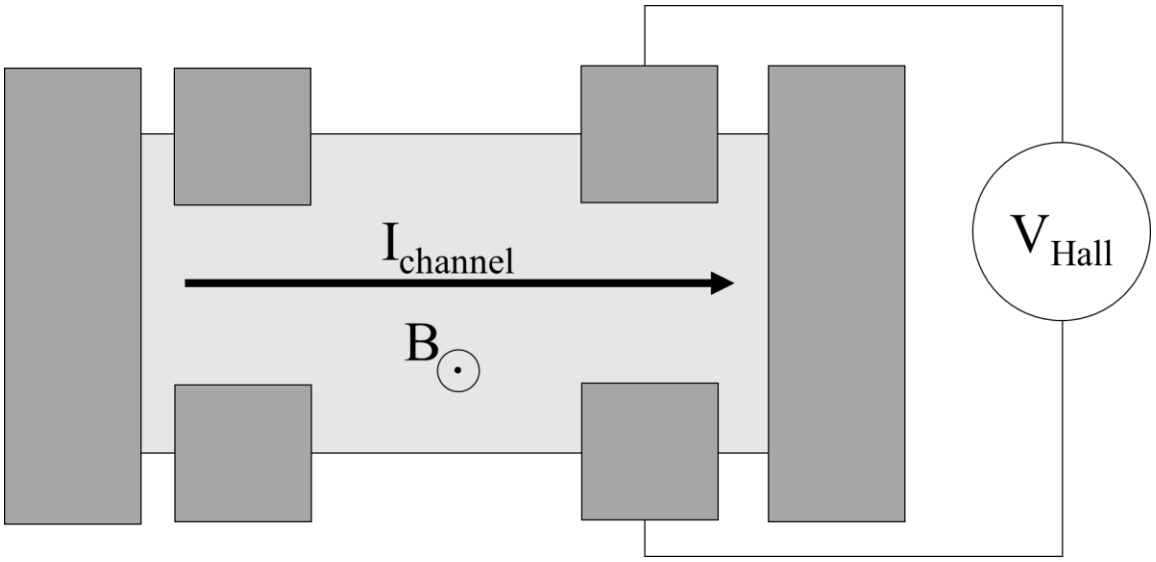

Figure 1.1 Schematic of a Hall voltage measurement. Shaded regions represent Ohmic contacts.

1.2.2 Quantum Dots and Other Systems

Coulomb blockade thermometry in quantum dots (QD) are well known primary thermometer and a useful tool to characterize the electron temperature in a cryogenic system. Chapter 3 describes the use of a QD processed on an (Al)GaAs structure to characterize the electron temperature in an Oxford Instruments Triton 200 cryogen-free dilution refrigerator. In addition to (Al)GaAs samples, InAs and InSb are well known 2DEG materials studied cryogenic temperatures.

CHAPTER 2. OPTIMIZATION OF A CRYOGEN-FREE DILUTION REFRIGERATOR FOR LOW-TEMPERATURE MEASURMENTS

2.1 Introduction to Cryogen-Free Dilution Refrigerators

A cryogen-free dilution refrigerator, also known as a 'dry fridge', is a dilution refrigerator that does not require the addition of liquid helium-4 to the system during cool down. The term 'dry' comes about because instead of requiring liquid helium and a 1-K (1 kelvin) pot to cool the system below liquid helium temperatures, the system is cooled to 4 K using a pulse refrigerator (PTR). The sample space does not come in direct contact with any cryogens, rather the sample is thermally anchored to the mixing chamber (MC) which reaches temperatures of 10 mK. The dry fridge described in this thesis is an Oxford Instruments Triton 200.

A dry fridge offers several benefits over a traditional 'wet' dil fridge. Operators do not have to refill the helium-4 used during cool down, reducing the cost of operation. Samples can also be changed relatively quickly on a dry fridge. For instance, if the Triton 200 is already at base temperature a sample can be removed from the dry fridge and a new sample can be loaded and cooled to base temperature in about 24 hours. In contrast, a traditional wet dil fridge can take several days to change a sample and for the fridge to cool back down to base temperature. However, dry fridges are especially susceptible to vibrations due to the pulsing vibrations inherent in the PTR and great care must be taken to mitigate the effects of these vibrations on electronic measurements.

An optimized dilution refrigerator is an ideal cryogenic system to study the fractional quantum Hall effect. In very high quality two-dimensional electron gas (2DEG) semiconductor samples, like the (Al)GaAs structures grown via MBE measured here, the exotic fractional quantum Hall state of $\nu = 5/2$ is observed. At temperatures below 30 mK well-developed reentrance states are also observed in these high quality samples.

Coulomb blockade thermometry (CBT) in quantum dots (QD) are also of interest because QDs constitute a primary thermometer and as a result are a way to directly probe the effective electron temperatures of the system. See Chapter 3 for more details on QD thermometry.

Other measurements of interest to the Manfra Group that can be taken using the dry fridge are electron interferometry on (Al)GaAs heterostructures, along with InSd and InAs Majorana structures and superconductor-normal metal-superconductor (SNS) junctions.

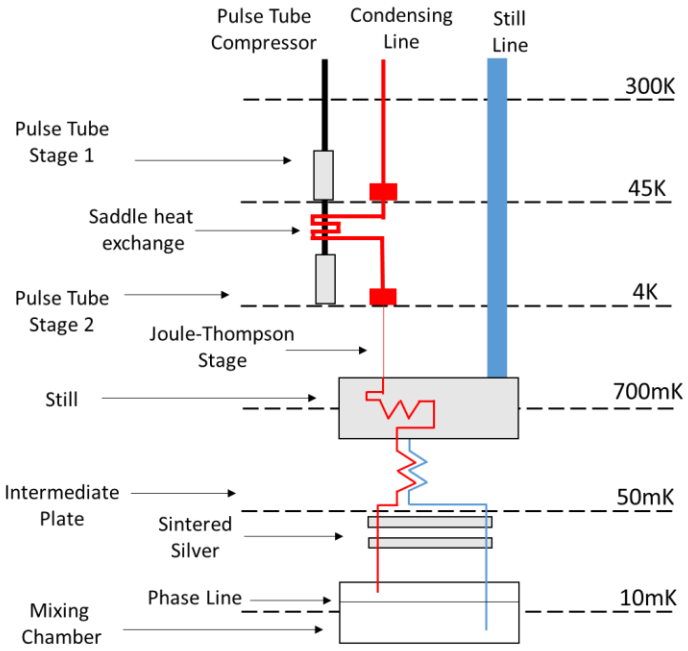

Figure 2.1 Schematic of the main components of a cryogen-free dilution refrigerator. The PTR is a closed system that utilizes helium-4 circulation to cool the fridge down to 4 K, with the path traced in black. The red components represent warm ^{3}He/^{4}He mix coming from the pump carts to the condensing line of the dilution unit, blue components represent cold ^{3}He preferentially evaporate by the still pumps.

The schematic in Figure 2.1 shows the main components of a dry dil fridge. The dilution unit works the same way in both a dry fridge and a conventional (wet) fridge with the still, sintered silver continuous heat exchanges, and the mixing chamber (MC) making up the essential components of the dilution unit. Warm ^{3}He/^{4}He mixture is driven into the condensing line by a compressor where the warm helium is precooled by heat exchanges with the different PTR stages. In a wet fridge, precooling of the helium mix is done via thermal contact with a ^{4}He bath and the use of a 1-K pot. A 1-K pot is a liquid helium cell that, when pumped on, allows for evaporative cooling of the liquid helium to temperatures of about 1 kelvin. The mix then passes through a narrow constriction which opens up to a larger diameter stage (Joule-Thomson) allowing the ^{3}He/^{4}He mixture to expand and form condensation. The liquid helium next passes through heat exchanges at the still (~700 mK) and intermediate plate (~50 mK) before moving through the sintered silver continuous heat exchanges which have a very large surface area to volume ratio and therefore an very large cooling power. Following the sintered silver the mixture enters the mixing

chamber where the ^{3}He and ^{4}He will separate at temperatures below 86 mK, with ^{4}He transitioning to a superfluid. The liquid ^{3}He can be passed through the ^{4}He superfluid and is pumped out of the still line where ^{3}He is preferentially evaporated. The heat exchange of the ^{3}He passing through the ^{4}He and evaporative cooling the superfluid allows the MC to get to temperatures of 10 mK.[1]

2.2 Initial Setup of Dry Fridge

2.2.1 Early Sample Cool Downs

During the initial cool down of the Triton 200, a doping well (Al)GaAs sample with a 195-nm deep 2DEG (measured from the surface), and a 75-nm setback between the 2DEG and the doping region (30 nm thick). The electron mobility μ is 31×10^6 $(cm^2/V\ s)$ with a 2DEG density n of $2.9 \times 10^{11}\ cm^{-2}$. This sample was chosen because it was well characterized in an Oxford Instruments Kevlinox wet fridge at applied MC temperatures from 10 mK to ~50 mK and showed well developed reentrant-integer quantum hall effect (RIQHE) at a filling factor of 2 which has been shown to be strongly temperature dependend.[5] The initial measurements of the sample inside the Triton looked very similar to the 50 mK data from the Kelvinox. The MC thermometer on the dry fridge was calibrated using nuclear orientation and is to be believed at temperatures of 10 mK, so it was clear that thermalization of the leads and electronic filters were required to bring the electron temperature closer to the MC at lowest temperatures.

2.2.2 Initial Thermalization of Electronic Measurement Leads

At extremely low temperatures the thermal resistance between the phonons of the lattice and the 2DEG of the sample is proportional to T^{-4}, resulting in very weak cooling powers between the sample mount and the electrons in the 2DEG.[6] This necessitates strong thermalization of the measurement leads in order to cool the electrons in the 2DEG. The Triton 200 was initially wired without the thermalization of the electrical leads as a priority. Constantan loom ran from room temperature down to the MC, with only brass L-bracket clamps to thermalize the electrical leads at the different cold plates. Constantan was used (as opposed to copper) because it is ~30x more resistive than copper at room temperature, resulting in less conduction of heat from room temperature and other warmer stages of the fridge down to the sample at the MC. However, if

proper heat sinks are installed at the coldest stages of the fridge, better conductors (like copper or silver) can be used to allow heat to dissipate on the cold plates, bringing the temperature of the electrons in the wires closer to the MC temperature.

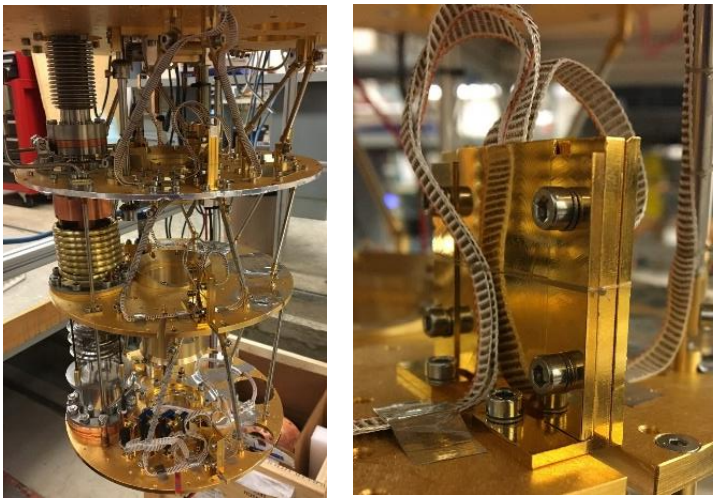

Figure 2.2 Initial wiring and thermalization of measurement leads. Two looms of 12 twisted pairs constantan loom ran from room temperature down to the MC with only brass L-bracket clamps about ~5 cm x 5 cm to thermalize the leads at each cold stage.

High frequency RF noise can also raise the electron temperature at the coldest stages of the fridge, and removing this noise near the sample can help reduce that effective electron temperature. In order to reduce the electron temperature in the dry fridge the decision was made to install better heat sinks at stages below 4 K and low-pass filters on the MC.

2.3 RC/RF Filtering

Early measurements had room temperature Pi-filters installed with a cut-off frequency of 4 MHz. These filters are commercially available filters built in to a DSUB (part # 56-721-003 from API Technologies) that were used in a DSUB to Fischer connector converter box. RF frequencies are known to cause heating in electrons in dil fridges and the attenuation of these MHz and above frequencies has been shown to decrease electron temperatures significantly.[7-8] It was determined cryogenic filters were required.

QFilters made by QDevil IVS are RF/RC multistage filters assembled on PCB boards placed inside gold plated copper housings. They are designed to easily stack on top of each other and mount onto Oxford Instruments cold plates, which made them a viable fit for the dry fridge. The cut-off frequencies of the RF pi-filters inside the QFilter are 5 GHz, 1.45 GHz, and 80 MHz and the RC cut-off frequencies are 1.3 MHz (R = 1200 Ohms, C = 100 pF) and 145 kHz (R = 50 Ohms, C = 2200 pF). The QFilters were placed on the MC plate, before the other thermalizers on the MC plate.

2.4 Oxygen-Free High Conductivity Copper Bobbins

Further cooling of the electrical leads were accomplished by installing oxygen-free high conductivity (OFHC) copper bobbins (posts) that the measurement leads could be wrapped around. The increase in surface area of the leads in contact with the different cold stages would allow for better thermalization at the lowest temperatures of the fridge (still plate and below). It was also determined that copper loom, instead of constantan, would be used at the MC to increase thermal conductivity at 10 mK. Large OFHC copper bobbins were designed to accomplish this, and at 60 cm tall with a 16 cm diameter about a dozen turns of loom were allowed to wrap around each bobbin and each loom would wrap around a bobbin on the still plate (~700 mK), intermediate plate (~50 mK), and the MC plate (~10 mK). After the bobbins were machined they were sonicated in toluene, acetone, and IPA for 5 minutes each. Then the cleaned the bobbins were sanded with 1500 grit sand paper, followed by 2500 grit sand paper until the surface was mirror-like (Figure 2.3). Polishing the side of the bobbin was important to make sure no sharp edges were present that could potentially short the electrical leads. Polishing the surface of the bobbin that makes contact with the cold plates of the dil fridge is imperative because it maximizes the surface area in contact with the cold plate, increasing the thermalization of the bobbin.

The bobbins were attached to the cold plates using threaded brass rods that screw in to tapped holes on the cold plates, with a brass nut clamping the bobbin down to the cold plates and a molybdenum washer between the nut and bobbin. Molybdenum was chosen as the washer material because of its relatively low linear thermal contraction constant compared to copper and brass (a zinc-copper alloy).[9] The idea here is that as the system cools to MC temperatures and the brass and copper contract, which would normally result in loosening of the threads of the brass rod from

the tapped holes, the molybdenum washer contracts much less and keeps the bobbin fixed tightly in place.

Table 2.1 Linear thermal contraction constants of relevant materials

Material	**Linear Thermal Contraction Constant** ($\mathbf{10^{-6}K^{-1}}$)
Molybdenum	4.8
Copper	16.5
Zinc	30.2

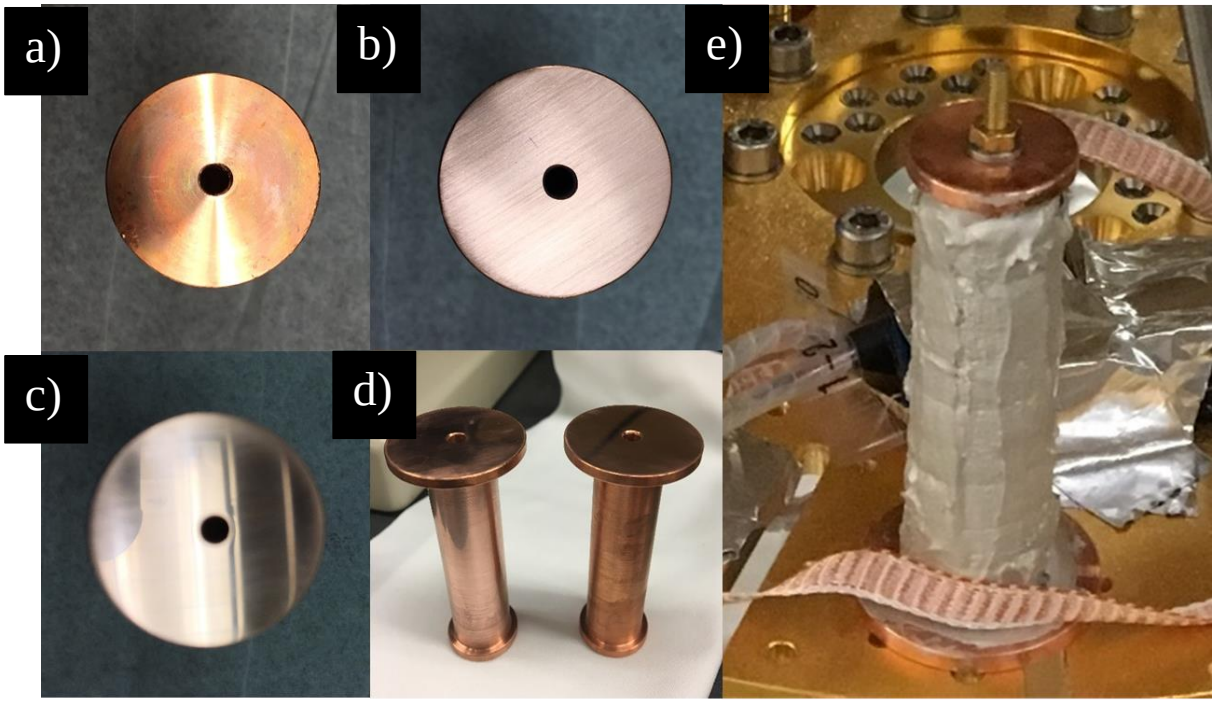

Figure 2.3 OFHC copper bobbins. a) Bobbin after cleaning in solvents b) after sanding with 1500 grit sandpaper c) after sanding with 2500 grit sandpaper d) left is a polished bobbin and right is an unpolished bobbin e) completed bobbin placed on the MC plate

The first attempt of the bobbins used silver epoxy (part # EJ2189-LV from Epoxy Technology) on all of the bobbins. However the solvents in the silver epoxy corroded the insulation on the constant loom which was used on the still plate and intermediate plate, but did not have

adverse effects on the copper loom insulation. The bobbins on the still plate and intermediate plate were stripped of loom and re-sanded. Then cigarette paper was placed between the loom and the bobbin and GE Varnish (part # VGE-7031 from Lakeshore Cryogenics) was used as a thermally conductive adhesive on the constantan loom, instead of silver epoxy. See Appendix A for recipe details.

2.5 Sapphire Meander Lines

For greater thermalization of electrons at the MC plate, gold meander lines deposited on sapphire substrates housed in OFHC copper boxes were designed based on thermalization boxes from.[10] Sapphire was used because of its unique properties of simultaneously being a good thermal conductor and good electrical insulator. The gold meander lines were deposited using photolithographic methods based on processes described in John Watson's thesis.[11] The sapphire substrate was glued on a specially designed OFHC copper box with a layer of silver paint (part # 16045 – Pelco 187 silver paint from Ted Pella, Inc) between the sapphire substrate and OFHC copper box. To hold the sapphire in place mechanically, an OFHC press plate and lid cover the sapphire and are clamped in place using brass threaded rod and brass nuts. A layer of Kapton tape was placed between the press plate and sapphire meander lines to make sure the lines were not shorted together. See Appendix B for more details.

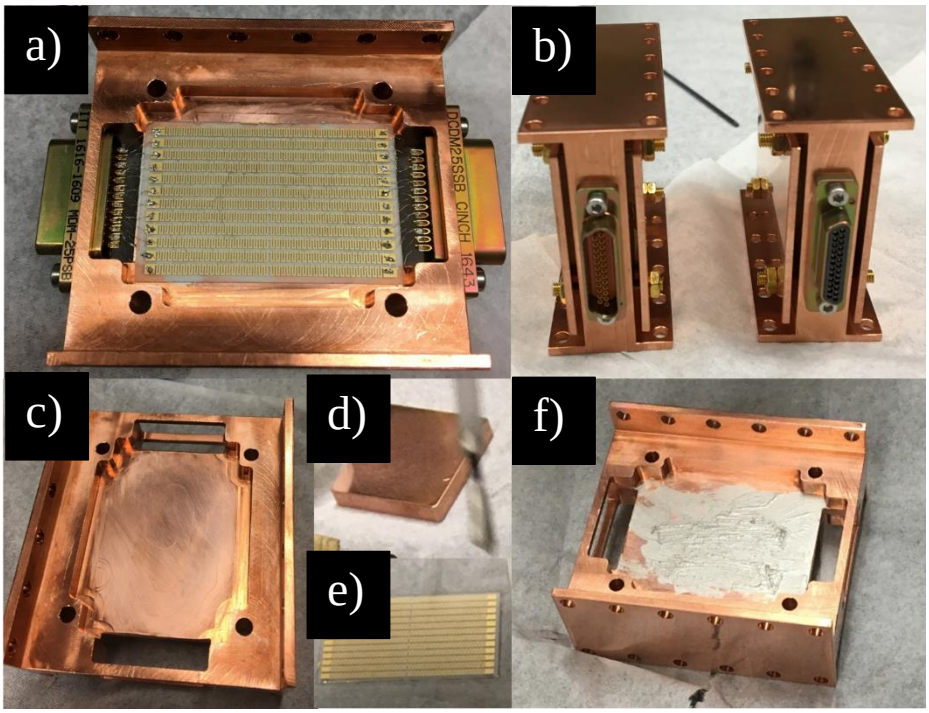

Figure 2.4 Gold meander lines on sapphire substrates housed in OFHC copper boxes. a) sapphire wafer pasted into OFHC copper housing b) assembled box with press plate and lid on top of the sapphire substrate c) cleaned ad sanded OFHC copper housing d) OFHC copper press plate e) sapphire substrate with gold meander lines deposited on surface f) OFHC copper housing with silver paste just prior to sapphire substrate being placed inside

2.6 Reduction of Vibrations Propagating to the Cryostat

Several sources of vibrations were found to propagate to the cryostat; pumps that control the helium mix circulating through the dilution unit, the PTR system, and indiscriminate vibrations through the frame of the cryostat. The original frame of the dil fridge was assembled out of aluminum extrusion using a minimalist approach. The rectangular frame extends across a trench in the floor of the lab that is ~4 meters long, while the shorter side of the frame is ~ 1 meter long. These dimensions allowed the early version of the frame to remain swaying for over 5 seconds if pushed or bumped; reinforcements were clearly required. Cross beams were added to the right-angles in the frame and across the longest sides of the frame, and new feet with a larger surface area were installed.

Vibrations from the circulation pump carts could be felt propagating from the pumps through the still line to the cryostat. The first attempt to mitigate these vibrations involved installing a U-bolt clamp on the still line attached to extrusion connected to the ceiling of the lab. This seemed to improve the Hall trace data some, but a more robust solution was deemed necessary. Ultimately a wooden box was built and rigid vacuum lines were added to the still line and passed through the box with about 150 kg of sand filling the box around the vacuum lines in order to dampen the vibrations. This is very similar to the sandbox implemented on the Kelvinox system in the Manfra lab, just on a much larger scale, and was deemed a success.

The pulse tubes refrigerator (PTR) was also determined to be a major source of vibrations. Although the PTR has no moving parts inside the cryostat, outside of the cryostat there is a rotary motor that regulates the flow of high pressure and low pressure helium-4 in the PTR at a frequency of 1.4 Hz. This motor was mounted directly onto the top plate of the cryostat, effectively sending mechanical vibrations of 1.4 Hz throughout the fridge. Reservoirs for the 45 K and 4 K pulse tube stages were also directly mounted on the cryostat. To decouple the vibrations propagating from the PTR components to the cryostat a secondary frame was built across the cryostat to house the PTR rotary motor and reservoirs. Several other iterations of vibration dampening of the PTR were tried before the frame was installed. Sorbothane vibration dampening foam was placed between the rotary motor and the cryostat top plate. Although the vibrations detected on the cryostat were reduced, this did not seem to affect the quality of the Hall transport data nor did it lower the estimated electron temperature. This lead to the design and implementation of the secondary frame.

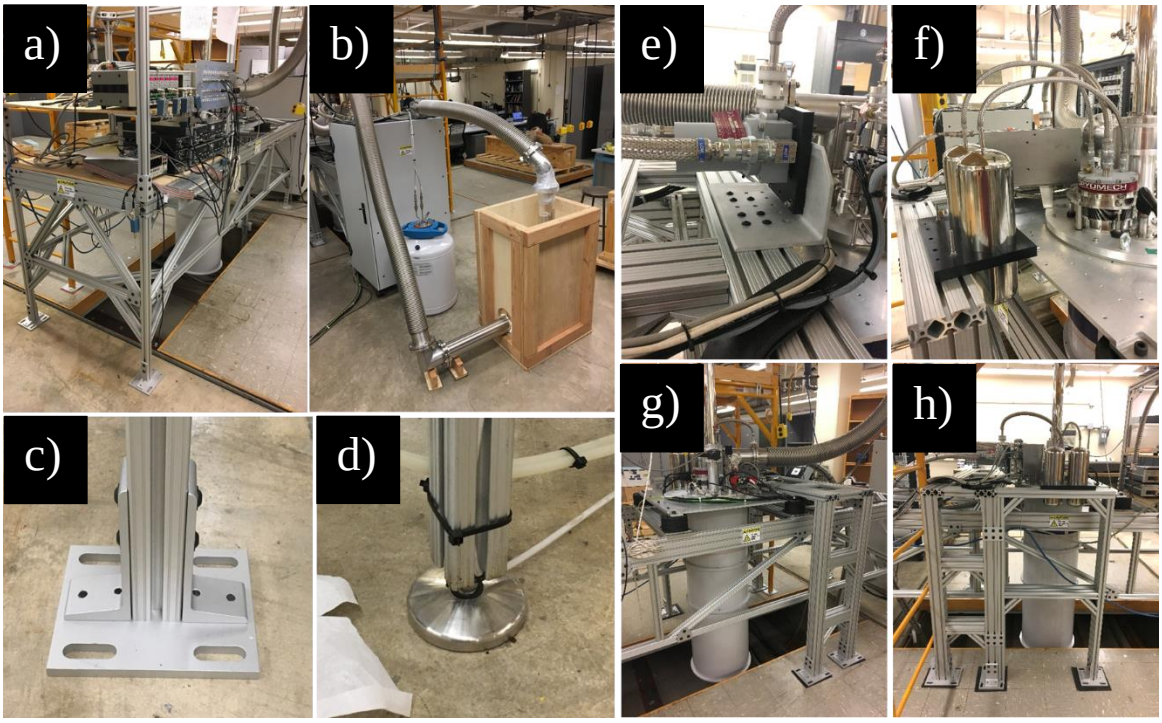

Figure 2.5 Mechanical upgrades to the dry fridge. a) Frame after cross braces and new feet were installed b) still sand box c) upgraded feet d) old feet e) PTR rotary motor on new mount and frame f) PTR reservoirs on new frame g) new PTR frame on measurements side of frame h) new PTR from h) new PTR frame on reservoir side of frame

2.7 Puck Upgrades

The initial puck design had electrical leads insulated with a Teflon coating floating from the sample socket to the nano-D connectors that mate the puck to the MC. The sample socket was initially a silver plate that was thermally connected to the rest of the puck via braised silver wires from the silver plate to the chamber of the puck, and four stainless steel rods connecting the same areas, this left much room for improvement. A new puck consisting of OFHC copper and a built in clamp was designed based on the Kelvinox tail shown in John's thesis.[11] The puck was machined and wired up at Oxford Instruments in the UK. Upon arrival at Purdue the puck was wiped down with IPA and clean wipes three times before adhesive was added to the wires passing through the clamp. The conductive adhesive used was a 50:50 mixture by mass of GE Varnish and silver powder (part # 61-310 from Ted Pella, Inc). The recipe used is detailed in Appendix C.

Figure 2.6 new clamping puck with GE-Varnish and silver powder mixture. Left, new clamping puck with copper loom passed through clamp and mixture of GE-Varnish and silver powder coating the copper loom and on the right is freshly mixed GE-Varnish and silver powder slurry

2.8 Conclusions

After the frame upgrades, decoupling the PTR components from the cryostat, installation of the QFilters, bobbins, and sapphire meander lines, along with the redesign of the sample puck the Hall transport data gave clear indication of a decrease in electron temperature. The largest improvement in electron temperature was seen with the use of the new puck, however it is unclear that if the upgrades were done in a different order what the true limiting factor would have been.

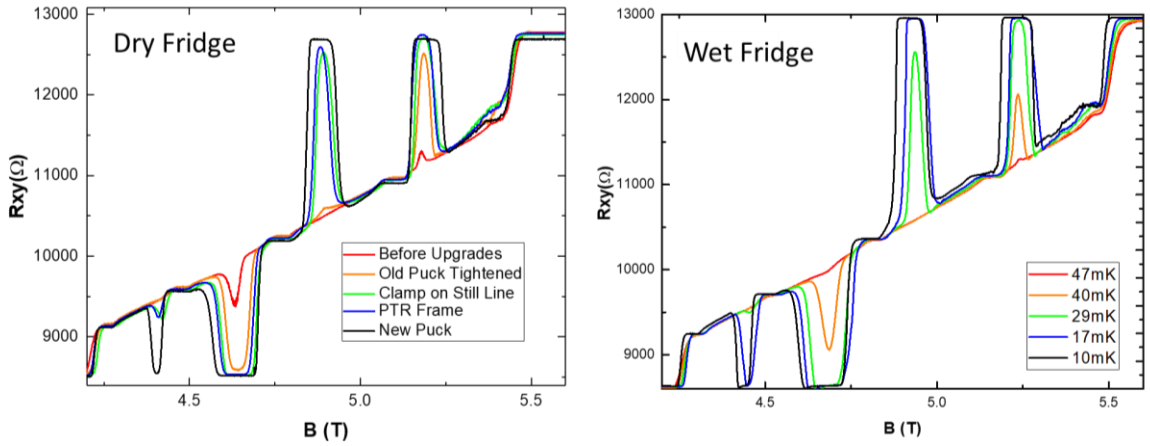

Figure 2.7 Hall measurements comparing the same Van der Pauw square sample measured in the dry fridge and the wet fridge. Dry fridge upgrades are compounding and traces include all the upgrades stated above them. Wet fridge measurements were done with applied heat to the MC.

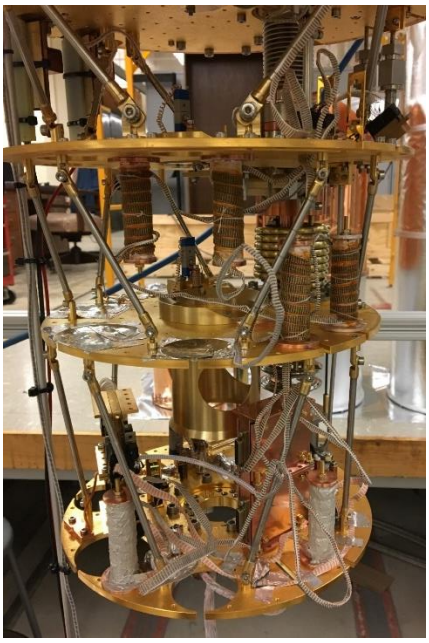

Figure 2.8 Picture of MC, intermediate, and still plates after bobbins, sapphire meander lines, and QFilters were installed.

After the upgrades were implemented, the magnetotransport data looks most similar to the data taken in the wet fridge at a MC temperature of 17 mK, with some well -developed RIQHE features In contrast, there is very little development of RIQHE features in the trace taken before upgrades to the Triton 200 were made.. However, this does not suggest the electron temperature is in perfect agreement with the MC temperature at 17 mK, in fact we would expect the electron temperature to be warmer than the MC (see Section 2.2.2). The Hall transport is still a useful tool to estimate the electron temperature at ~20 mK, especially when looking at the development of the re-entrance states. Clearly improvements in the electron temperature of the sample have been made, but the electron temperature must be probed directly to understand what further optimization is needed to bring the electron temperature as close to the MC temperature as possible.

CHAPTER 3. QUANTUM DOTS

3.1 Introduction to Quantum Dots

Quantum dots (QD) constitute a well-known primary thermometer, making them an ideal candidate to probe the effective electron temperature of the dry fridge.[12-16] A quantum dot is a device that confines electrons in a region small enough to make quantum mechanical energies scales observable (Ihn, 2010). This can be done via metal gate deposition on the surface of a semiconductor material with a well-defined two-dimensional electron gas (2DEG). The electron island is defined via quantum point contacts (QPCs) tuned to barely conduct. QPCs are split gates with a narrow gap of a similar length scale to the Fermi-wavelength of the electrons in the system. When negative voltages are applied to the gates, depleting the 2DEG beneath them, the conductance through the QPC becomes exactly quantized at values of $2e^2/h$, known as the conductance quanta G_0.[17] When negative enough voltages are applied to the gates the effective width of the QPC is zero and there is no allowed current through the QPC, this is called pinch-off.

To determine the electron temperature of a QD three measurements must be taken; QPC conductance plateaus in order to roughly tune the QPCs, Coulomb blockade conductance peaks to finely tune the QPCs, and Coulomb blockade diamonds to extract the lever arm (α) of the plunger gate. Coulomb blockade is one of the defining characteristics of a quantum dot, it is defined by the increase in resistance at small bias voltages of devices with tunnel junctions that have small capacitances, e.g. quantum dots. The effect arises in devices that are small enough that electron-electron interaction within the device create strong Coulomb repulsion which prevents the flow of electrons. Oscillating regimes of electron flow occur when the source drain voltage (V_{SD}) is increased or the plunger gate voltage (V_P) is varied (see Figure 1 b and c). The island is defined by QPCs and other metallic gates on the surface of the semiconductor (see Figure 1a). Applied voltages to these gates deplete the 2DEG beneath the gates and effectively isolate the electrons in the dot from the bulk 2DEG. The QPC gates are tuned (negative voltages are applied symmetrically across the QPC gates) such that they become tunnel barriers, allowing for a single electron to hop onto or off of the confined electron island. This effect is called Coulomb blockade, and is observable by measuring the source-drain current while varying the plunger gate voltage with the QPCs tuned properly.

Another important measurement taken in quantum dots is the Coulomb blockade diamond. This is taken by sweeping V_{SD} and V_P while measuring the current through the dot. This leads to diamond patterns in the data that signify regions of high conductance (outside the diamond) and zero conductance (inside the diamond). This measurement gives the lever arm of the plunger gate, which is a proportionality constant describing the ratio of the capacitance of the plunger gate to the total capacitance of the QD. In more intuitive terms it describes the effect of changing the charge of the plunger gate on the charge of the QD.

At temperatures near absolute zero and length scales of a few hundred nanometers there are a few energy scales that are very important. The Coulomb energy, sometimes referred to as charging energy (E_C), describes the energy it takes to add an electron to the island by overcoming the tunnel barriers of the QPCs. Level spacing (ΔE) describes the energy it takes for an electron on the island to move to the lowest order excited state. Source-drain coupling, or tunneling rate (Γ), describes the rate at which electrons escape from the island. And finally thermal energy (kT), which is near the level spacing in terms of energy scales at temperatures below 1 K and for quantum dots smaller than a micron or so. A linear relationship between temperature, the lever arm, and the FWHM of a conductance peak allows for a quantum dot to be considered a primary thermometer. The relationship of which is described in Equation 3.5.

$$E_C = e^2/2C$$

Equation 3.1 Charging energy. E_C is the charging energy, e is the elementary charge of an electron, and C is the geometric capacitance of the QD. The charging describes the energy required to add an electron to the quantum dot.

$$\Delta E = \frac{\hbar^2 \pi}{m^* L^2}$$

Equation 3.2 Single particle level spacing. ΔE is the level spacing, $\hbar$ is Planck's constant, m^* is the effective mass of the electron ($0.067m_0$ in GaAs) and L is the length of the quantum dot. This is the energy it costs to move an electron in the dot to the lowest order excited state. Using this particle-in-a-box approximation, the level spacing of a 100 nm QD is ~360 μeV.

$$kT = 0.86\ \mu eV\ at\ 10mK$$

Equation 3.3 Thermal energy. k is Boltzmann's constant and T is temperature. At MC temperatures of 10 mK the thermal energy is $\sim 1\ \mu eV$

Another parameter important in the ultra-low temperatures of a dilution refrigerator and the nanometer length scales of a QD is the tunneling rate Γ. This is the rate at which a confined electron escapes from the dot to the bulk 2DEG. The energy associated with the tunneling rate is assumed to be small compared to the charging energy, thermal energy, and level spacing.

There are two electron transport regimes a quantum dot can exist in; multilevel and single-level. The multilevel regime, sometimes referred to as the classical transport regime, is the regime in which the thermal energy is larger than the level spacing in the dot ($E_C > kT > \Delta E$). The single-level transport regime occurs in very small semiconductor QDs and is defined as the regime where the level spacing is larger than the thermal energy ($E_C > \Delta E > kT$). At temperatures of 10 mK a 500 nm QD, like the one measured here, is expected to be the in single-level transport regime ($\Delta E \cong 14\ \mu eV$).

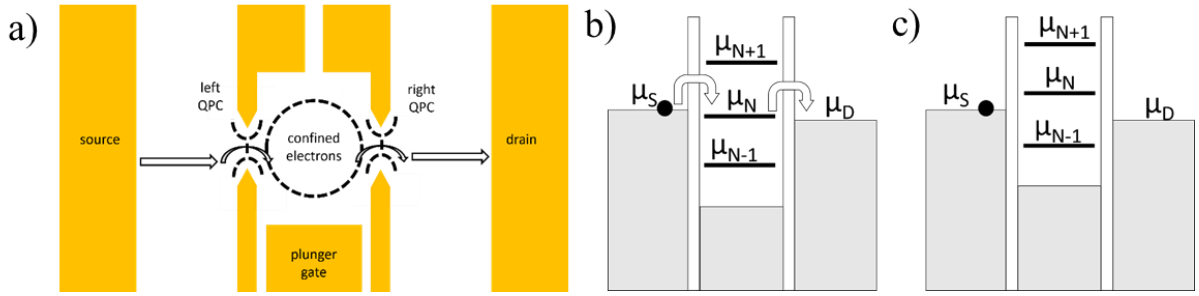

Figure 3.1 a) Schematic drawing of a split gate QD design. Solid white arrows represent the path of the electrons. The confined electrons are defined by the dotted region in the center of the dot, and the dotted regions around the QPCs represent the tunnel barriers after the QPCs have been tuned b) energy scale diagram of a QD in the high conductance regime c) represents the regime with no conductance.

3.2 Quantum Dot Design

The wafer chosen for this QD device is similar to wafer A in Ref. 9, chosen because of its low electronic switching noise and low conductance drift properties.[18] The wafer is a uniformly doped single-interface heterostructure with a 90-nm deep 2DEG (measured from the surface), and a 45-nm $Al_{0.36}Ga_{0.64}As$ spacer between the 2DEG and the doping region (11.5 nm thick). The electron mobility μ is 5.0×10^6 $(cm^2/V\ s)$ with a 2DEG density n of 1.7×10^{11} cm^{-2}.

The quantum dot measured in these experiments was lithographically defined using a combination of standard photolithography and electron-beam lithography techniques described in John Watson's thesis.[11] The metallic gates that define the quantum dot are Ti/Au (10 nm /15 nm) with an effective confined area of ~0.200 μm^2 (diameter of 400 nm).

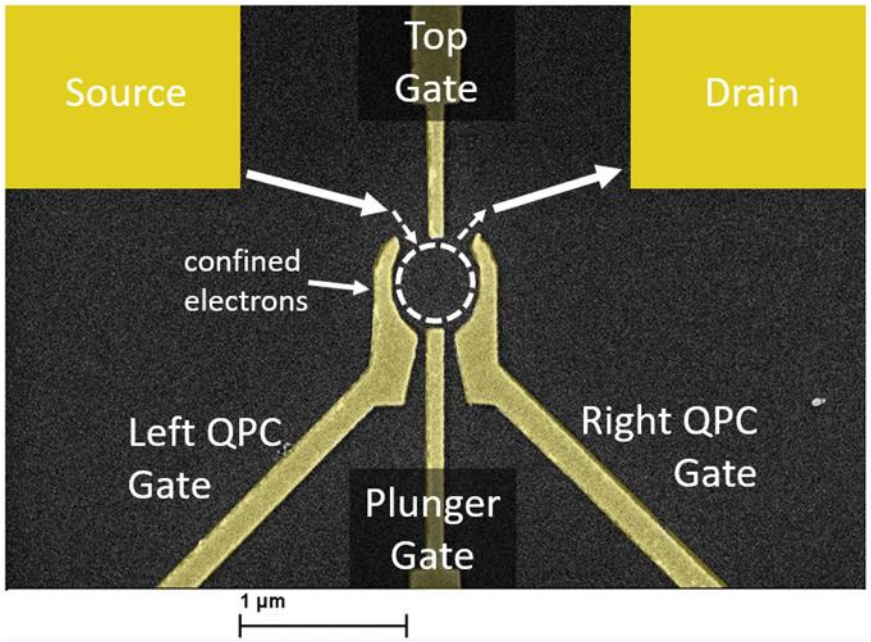

Figure 3.2 SEM image of a quantum dot similar to the one measured. Metallic gates are colorized in gold with Ohmic source and drain contacts represented as the rectangles in the upper left and right corners. The arrows represent the path of electrons from source to drain with the dotted arrows representing tunneling electrons. The dotted circle in the middle of the gates represents the electrons confined in the QD when the dot is properly tuned.

Figure 3.2 shows an SEM image of a QD similar to the one measured here. Ohmic contacts on either side of the QD constitute the source and drain of the device. QPCs are defined between the top gate and right and left QPC gates, respectively. The plunger gate is capacitively coupled to the confined electrons in the QD; varying the voltage on the plunger gate changes the allowed energy states of the confined electrons and allows for conductance resonance peaks, see Figure 1 b and c.

3.3 Quantum Dot Measurements

3.3.1 QPC Conductance Plateaus

The goal of these QD measurements was to extract the electron temperature of the dry fridge after the upgrades in Chapter 2 were implemented. Before the Coulomb blockade diamonds and conductance peak measurements can be taken the QPCs must be tuned. This is done by sweeping the individual QPCs from zero applied voltage to more negative voltages, until the QPCs are no longer conducting; this is called pinch-off. The conductance through the QPCs is exactly quantized to integer values of $2e^2/h$ as the QPC voltages approach pinch-off.

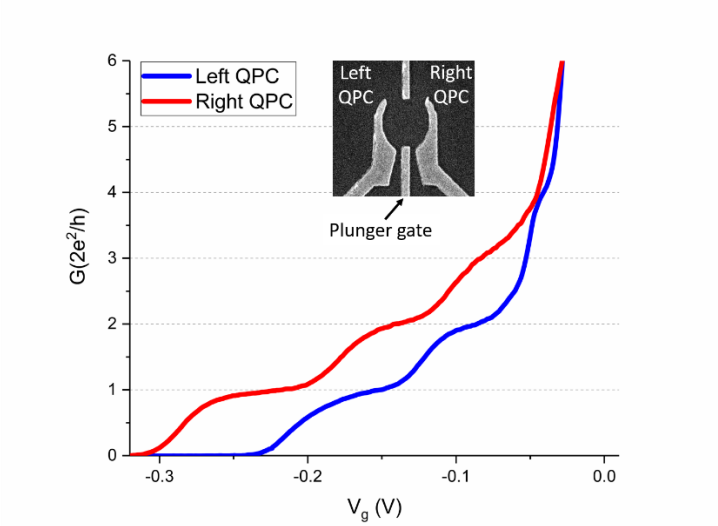

Figure 3.3 Conductance through the QPCs as a function of applied gate voltage. Measurements were taken with -200 mV applied to the top gate and +300 mV applied to the QPC gate that was not being measured so as not to impede the electron path of the QPC being measured. Inset: SEM image of a QD similar to the one measured

Both QPCs show developed plateaus at the lowest integer values of the conductance quantum G_0. By tuning both QPCs near pinch-off the QPCs act as tunnel barriers and effectively trap electrons inside the QD, isolating these electrons from the source and drain of the device.

3.3.2 QD Conductance Peaks

Conductance peaks are measured by tuning the QPCs to the point just before pinch-off such that the measured current through the QD is zero, however by sweeping the plunger gate voltage peaks arise in the current through the QD. These regions of relatively high current can be converted to differential conductance (dI/dV_{SD}), consequently the measured current peaks are a way of probing the conductance through the dot. For QD in the single-level transport regime, conductance peak data can be fit to the following equation, and the FWHM of the peak can be determined:

$$G = \frac{G_{peak}}{cosh^2\left[\alpha(V_P - V_{peak})/2kT\right]}$$

Equation 3.4 Conductance peak formula. G_{peak} is the peak conductance value, V_P is the plunger gate voltage, V_{peak} is the plunger gate voltage associated with G_{peak}, α is the lever arm of the plunger gate, k is Boltzmann's constant, and T is the electron temperature.

A more thorough explanation of the peak conductance is explained in *Semiconductor Nanostructures* which contains the tunnel rate of the QPCs of the QD.[19] However, G_{Peak} can be determined through experimental data and the tunnel rates were not of direct interest to this project, therefore just using the experimental G_{Peak} was sufficient.

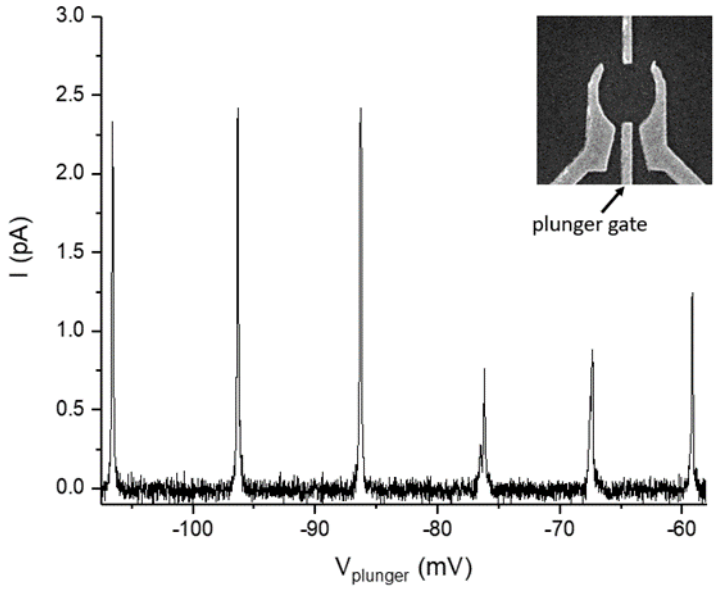

Figure 3.4 Conductance peaks measured by sweeping the plunger voltage after properly tuning the QPCs.

The peaks correspond to the states in Figure 3.1 b (high conductance) and the valleys correspond to the states in Figure 3.1 c (no conductance). Fitting an individual peak to the conductance peak Equation 3.4 allows for a full width at half maximum (FWHM) of the peak to be extracted. This value, along with the lever arm α of the QD, can be used to extract the electron

temperature of a QD in the single-level transport regime via the following linear relationship in Equation 3.5. In the case of multilevel transport, the slope on the right hand side of Equation 3.5 is scaled to 4.35 instead of 3.53 and Equation 3.4 can still be used to determine the FWHM.

$$\alpha FWHM = 3.53kT$$

Equation 3.5 Temperature extraction of Coulomb blockade peaks. Where α is the lever arm of the plunger gate, FWHM is the full width half at half maximum of the conductance peak found via Equation 3.4, k is Boltzmann's constant, and T is the electron temperature.

3.3.3 Coulomb Blockade Diamonds and Temperature Extraction

In Figure 3.5, the side of the peak with more positive $V_{Plunger}$ fits the expected line shape while the more negative $V_{Plunger}$ side is more Lorentzian, suggesting some additional asymmetric broadening on this device. The source of this broadening is unclear at the moment. Adding low pass filters with a cutoff frequency below 20 Hz to the source and drain of the device did make the conductance peaks less asymmetrical and less Lorentzian. This suggests there is noise being picked up in the measurement instruments, although it is unclear whether or not the noise is being injected into the QD or if it is just noise in the measurement circuit.

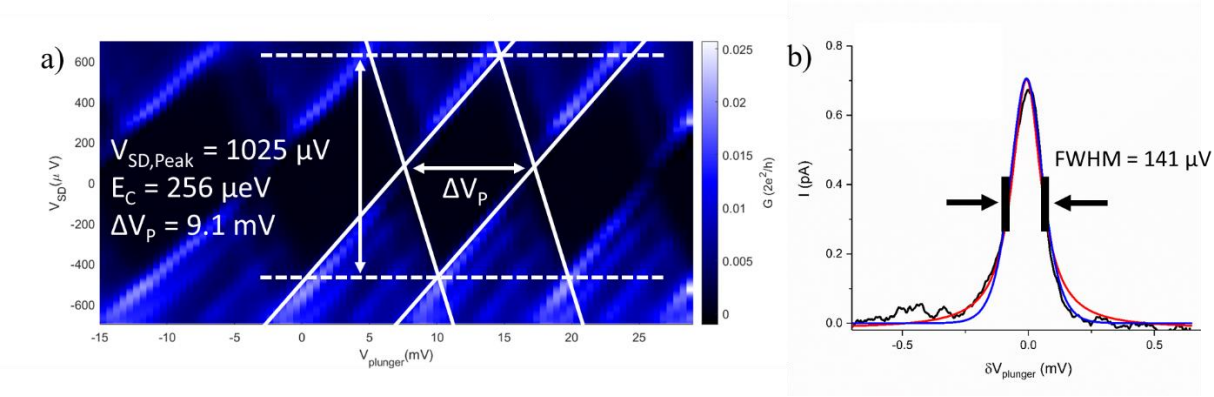

Figure 3.5 Coulomb blockade diamonds and conductance peak fitting. a) Coulomb blockade diamond plot taken by sweeping the source-drain voltage (V_{SD}) then stepping the plunger gate voltage ($V_{Plunger}$). The dark regions represent no conductance while light regions represent high conductance. The peak to peak source-drain voltage correlates to the charging energy (E_C) by a factor of 4/e where e is the electron charge. The period of the plunger gate voltage can also be determined from this measurement, giving the lever arm α of the plunger gate. b) Form fitting of a conductance peak. The blue line represents fitting of the peak to Equation 3.4. A Lorentzian line shape (red) representing a broadened peak is also plotted.

The combination of Coulomb blockade diamond plots and conductance peak measurements allow for the electron temperature to be extracted using Equation 3.5 and α calculated using Equation 3.6.

$$\boldsymbol{\alpha = \frac{\left|eV_{SD,peak}/2\right|}{\Delta V_p} = \frac{2E_c}{\Delta V_p}}$$

Equation 3.6 Lever arm of the plunger gate. α is the lever arm, e is electron charge, $V_{SD,peak}$ is the peak to peak source-drain voltage of the diamonds, E_C is the charging energy, and ΔV_P is the plunger gate voltage period.

Using Equations 3.4 through 3.6 and assuming single-level transport, the electron temperature is 25.0 mK. Fitting the temperature to the multilevel transport form the electron temperature is 20.3 mK.

To better determine whether the QD is in the multilevel transport or single-level transport regime the FWHM must be plotted as a function of temperature. This can be done by applying heat to the MC of the fridge, allowing the fridge to thermalize at the applied temperatures, and taking conductance peak sweeps at various temperatures.

3.3.4 Temperature Dependence of Conductance Peaks

To study the effects of applied heat on the conductance peaks, constant power was applied to the mixing chamber of the Triton 200 and conductance peak sweeps were taken from base temperatures up to 200 mK. The QPCs were retuned twice during these measurements which may have had an effect on the slope of the FWHM data. The retuning occurred around 100 mK and 50 mK. Retuning the QPCs changes the electrostatics of the QD and therefore shifts the location of the conductance peaks in terms of $V_{Plunger}$. Due to this effect from retuning the same it was virtually impossible to track the same peak before and after retuning.

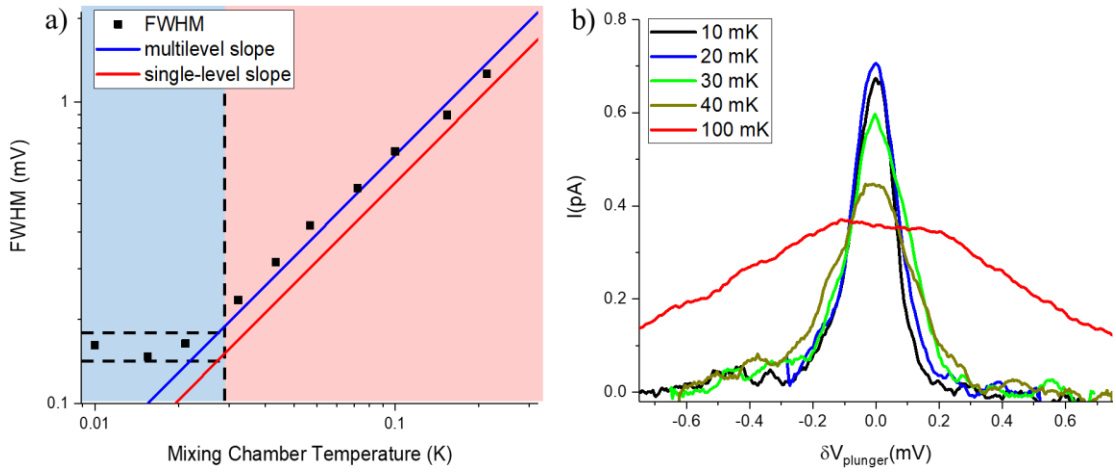

Figure 3.6 The effects of applied heat to the mixing chamber on conductance peaks. A) FWHM plotted at various MC temperatures below 200 mK. The data follows the multilevel transport slope well at temperatures above 30 mK, below 30 mK the FWHM saturates. B) Conductance peaks plotted at various temperatures. The peaks clearly broaden at increased temperatures.

The conductance peak measurements were taken at various temperatures between base temperature and 200 mK. Figure 3.6 a clearly shows the FWHM following the multilevel slope at warmer temperatures. This is somewhat unexpected due to the approximate level spacing calculated using the particle in a box Equation 3.2 ($\Delta E \cong 15\ \mu eV$, $kT \cong 1\ \mu eV$), therefore we would expect this dot to be the single-level regime at temperatures below $\sim 150\ mK$. However the calculated level spacing is just an approximation, which could explain the deviation of the empirical slope from the expected theoretical slope.

The decoupling of the FWHM from the mixing chamber is not unexpected at very low temperatures. Thermal resistance between the 2DEG and the phonons of the lattice scales proportionally to T^{-4} at low temperatures, leading to very weak cooling powers of the 2DEG through the lattice of the sample.[6] This is why cooling through the electrical leads via filtering and thermalization is required and described in depth in chapter 2.

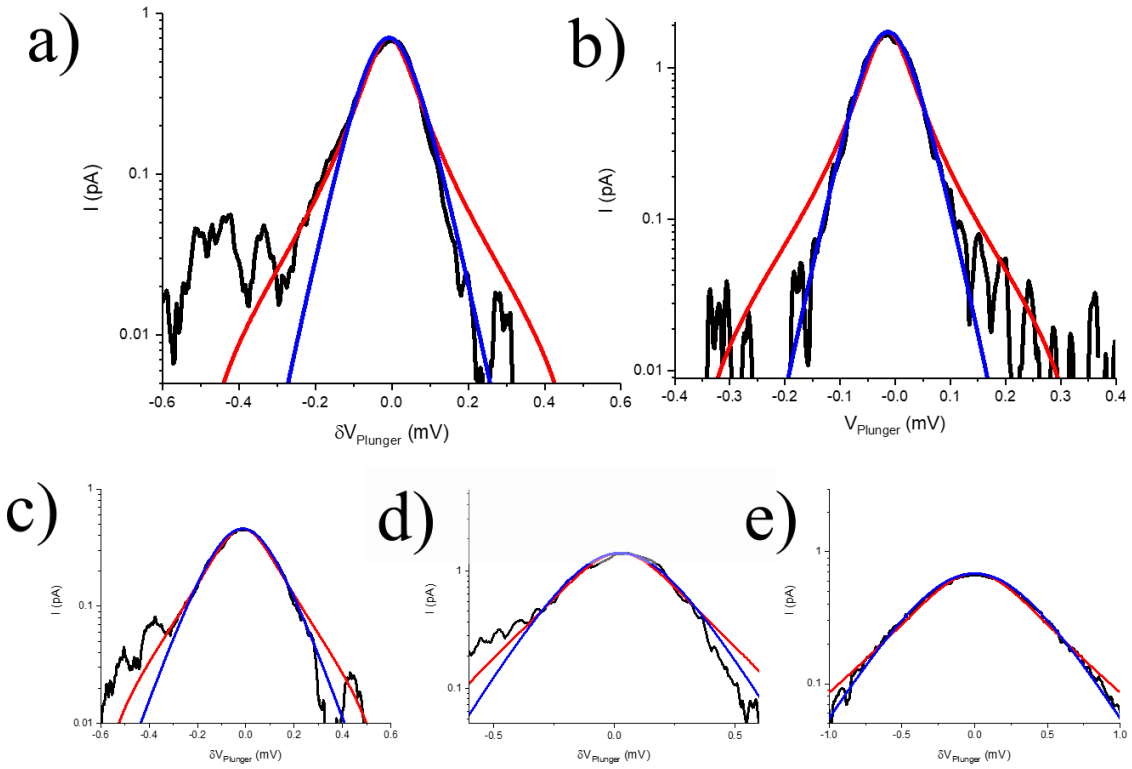

Figure 3.7 Line shape of peaks as a function of temperature and low-pass filtering. The black traces are the data, the blue traces are the fit from Equation 3.4, red are Lorentzian fits representing broadened peaks. a) Conductance peak at base temperature b) Conductance peak at base temperature with low-pass filters on the source and drain c) Conductance peak at a MC temperature of 40 mK d) Conductance peak at a MC temperature of 100 mK e) Conductance peak at a MC temperature of 150 mK.

The conductance peaks are a poor fit to the form in Equation 3.4 at temperatures of ~100 mK and below. Conductance peaks at base temperatures with (Figure 3.7 b) and without (Figure 3.7 a) LPFs in place on the source and drain of the device. The LPF data is less asymmetric then the non-filtered data. The conductance peak at base temperature without the LPFs in place (Figure 3.7 a) fit the Lorentzian line shape on the more negative $V_{plunger}$ side, while the more positive $V_{Plunger}$ side is a good fit to Equation 3.4.

At lowest temperatures the peaks are a poor fit to the form of Equation 3.4. This is due to some additional broadening, the source of which is yet unknown. Adding low pass filters on the source and drain of the QD did make the peaks fit a better fit to the expected line shape, however

at base temperature this did not affect the FWHM, therefore the extracted temperature remains the same. Data was not taken with applied heat to the MC with the low pass filters in place, so the effects of the LPF on the slope of the FWHM vs temperatures data is unknown.

3.4 Conclusions and Future Outlooks

Using the empirical multilevel transport slope the electron temperature of the system is 20.3 mK, which is in agreement with the estimated 20 mK from the quantum Hall data. Further temperature dependence measurements with the low-pass filters in place on the source and drain are needed to test if the conductance peaks continue to match the multilevel slope and if the line shape continues to agree with Equation 3.4 and remains symmetrical. Measuring the conductance peaks up to higher temperatures to observe whether or not there is a change in slope would also be useful. [20-21] It has also been suggested the slope of the temperature dependence can change from cool down to cool down.[7] A metallic island QD could be of interests to ensure the QD is in the multilevel regime.[3] The Manfra Group is also testing new InAs and InSb materials that could be used for QD fabrication.

APPENDIX A. OFHC COPPER BOBBINS

The following recipe was used when wiring up the OFHC copper bobbins. Future bobbins should be wound in non-inductively, unfortunately at the time the bobbins in the Triton 200 were made we were not aware of the benefits of this wiring scheme and we wired the bobbins inductively.

1. Sonicate the bobbins for 5 minutes each in toluene, acetone, and IPA. Rinse with methanol between each solvent stage
2. Polish top and bottom plate surfaces with 1500, then 2500 grit sand paper
3. Polish side of bobbin with 1500 then 2500 grit sand paper
4. Blow off excess dust with nitrogen gas or computer duster
5. Rinse with IPA
6. For MC plate bobbins:
    a. Coat side of bobbin with silver epoxy
    b. Wrap copper loom around tightly, tie with floss (or fishing line), then thoroughly coat loom in silver epoxy
7. For still and 100 mK plates:
    a. Wrap cigarette paper over bobbin and coat in GE Varnish
    b. Wrap constantan loom around tightly, tie with floss (or fishing line), then coat loom in GE Varnish
8. Let dry (48-72 hours) then check electrical leads for continuity and shorts

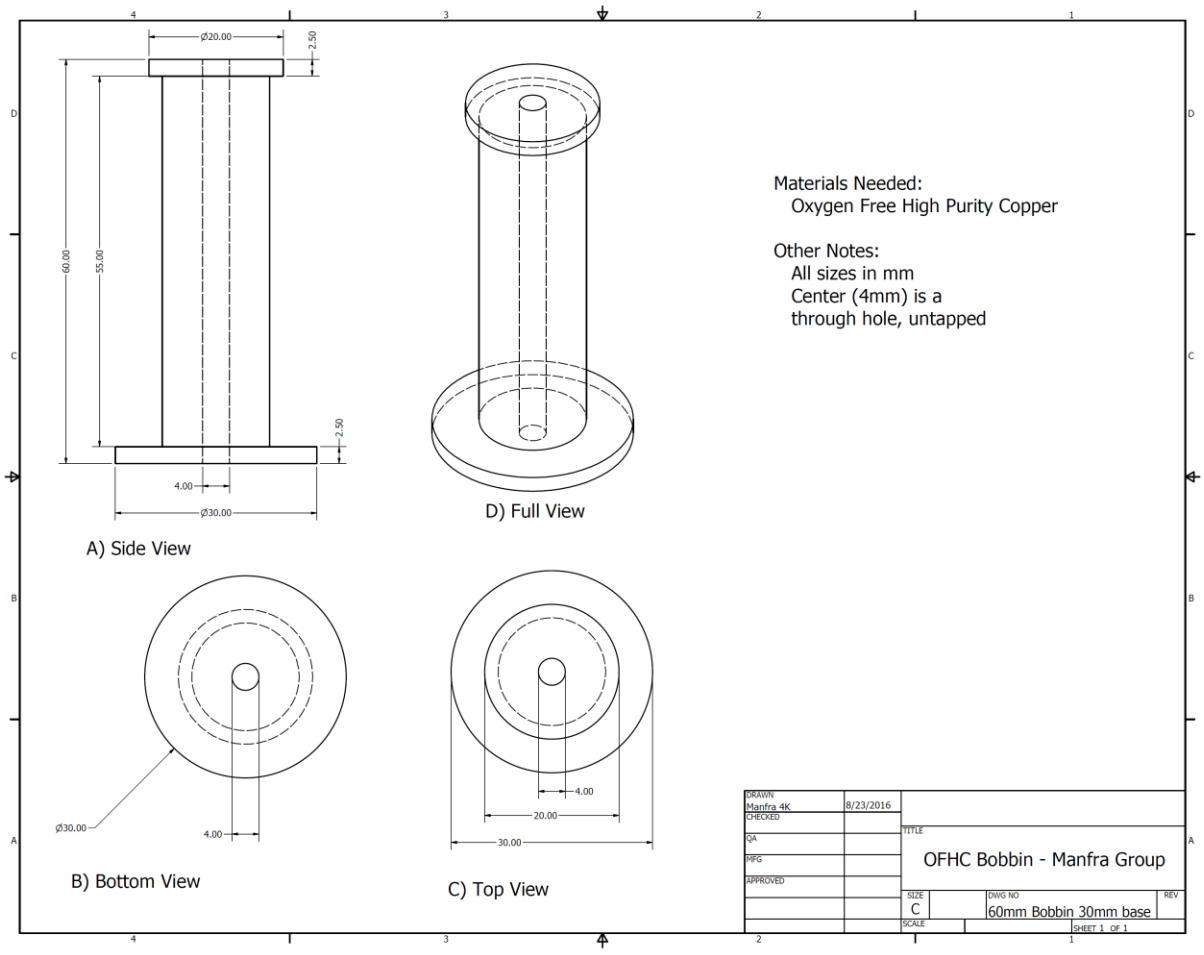
Ø20.00
2.50
60.00
55.00
2.50
4.00
Ø30.00
A) Side View
D) Full View
Materials Needed:
Oxygen Free High Purity Copper
Other Notes:
All sizes in mm
Center (4mm) is a
through hole, untapped
Ø30.00
4.00
B) Bottom View
4.00
20.00
30.00
C) Top View
DRAWN
Manfra 4K
8/23/2016
CHECKED
QA
MFG
APPROVED
TITLE
OFHC Bobbin - Manfra Group
SIZE
C
DWG NO
60mm Bobbin 30mm base
REV
SCALE
SHEET 1 OF 1

APPENDIX B. GOLD MEANDER LINES ON SAPPHIRE SUBSTRATES

Design of the OFHC copper box used to hold the gold meander lines on sapphire substrates.

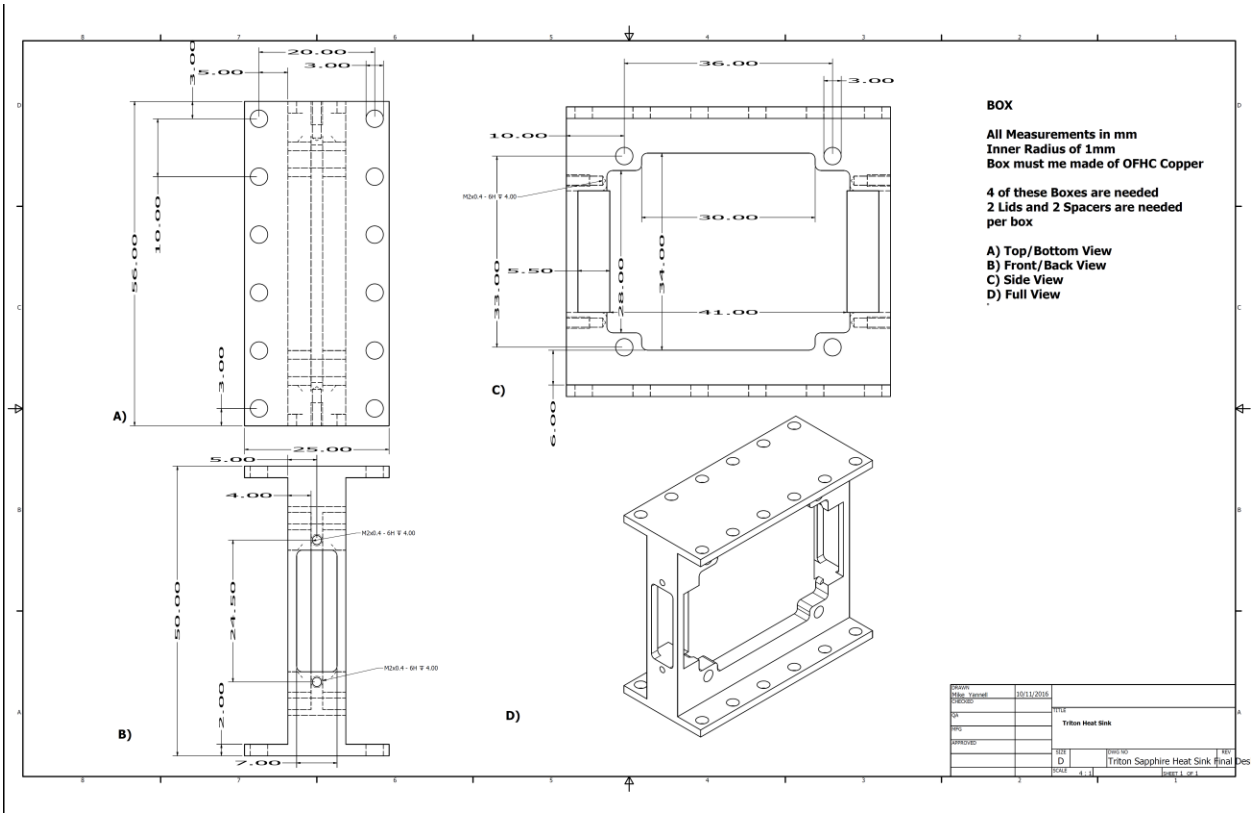

APPENDIX C. OFHC COPPER PUCK

After receiving puck from Oxford Instruments the below steps were taken.

1. Triple cleaned all surfaces that varnish will touch with IPA and Kimwipes
2. Covered all electrical socket and the base of the puck with Kapton tape and Kimwipes
3. Covered sample socket in Kapton tape
4. Put brass screws for clamp in TCE and let sit in order to lubricate when clamping down at the end of the potting process
5. Mixed ~10g of GE Varnish with ~10g silver powder
    a. Take 10g of varnish and add 1g of silver powder at a time, mix, repeat
    b. Varnish will go from rich translucent honey color to opaque
    c. Resistance of Varnish will start at ~1.5 MOhms per inch and drop to ~0.8 MOhms per inch when enough powder is added
    d. When dry the mix will have a resistance of a couple Ohms
    e. Use 1:1 mix of methanol and toluene to stretch the working life of the varnish
6. Put the varnish mix on the puck
7. Put loom over varnish
8. Add another layer of varnish mix on top of the loom
9. Put clamp in place and screw down
10. Let sit for ~72 hours before moving
11. Check all electrical leads

REFERENCES

1. Balshaw, N. H., *Practical Cryogenics An Introduction to Laboratory Cryogenics*. Oxford Instruments Superconductivity Limited: 1996; p 96.

2. Deng, N.; Gardner, G.; Mondal, S.; Kleinbaum, E.; Manfra, M.; Csathy, G., nu=5/2 Fractional Quantum Hall State in the Presence of Alloy Disorder. *Phys Rev Lett* **2014,** *112* (116804), 5.

3. Iftikhar, Z.; Anthore, A.; Jezouin, S.; Parmentier, F. D.; Jin, Y.; Cavanna, A.; Ouerghi, A.; Gennser, U.; Pierre, F., Primary thermometry triad at 6 mK in mesoscopic circuits. *Nature Communications* **2016,** *7*, 12908.

4. Manfra, M. J., Molecular Beam Epitaxy of Ultra-High-Quality AlGaAs/GaAs Heterostructures: Enabling Physics in Low-Dimensional Electronic Systems. *Annual Review of Condensed Matter Physics* **2014,** *5* (1), 347-373.

5. Watson, J. D.; Csáthy, G. A.; Manfra, M. J., Impact of Heterostructure Design on Transport Properties in the Second Landau Level of In SituBack-Gated Two-Dimensional Electron Gases. *Physical Review Applied* **2015,** *3* (6).

6. Baer, S.; Ensslin, K., *Transport Spectroscopy of Confined Fractional Quantum Hall Systems*. 2015; Vol. 183.

7. Mueller, F.; Schouten, R. N.; Brauns, M.; Gang, T.; Lim, W. H.; Lai, N. S.; Dzurak, A. S.; van der Wiel, W. G.; Zwanenburg, F. A., Printed circuit board metal powder filters for low electron temperatures. *Rev Sci Instrum* **2013,** *84* (4), 044706.

8. Scheller, C. P.; Heizmann, S.; Bedner, K.; Giss, D.; Meschke, M.; Zumbühl, D. M.; Zimmerman, J. D.; Gossard, A. C., Silver-epoxy microwave filters and thermalizers for millikelvin experiments. *Applied Physics Letters* **2014,** *104* (21).

9. Ekin, J., *Experiment Techniques for Low-Temperature Measurements*. 2006; p 704.

10. Kou, A. Microscopic Properties of the Fractional Quantum Hall Effect. Harvad University, 2013.

11. Watson, J. D. Growth of Low Disorder GaAs/AlGaAs Heterostructures by Molecular Beam Epitaxy for the Study of Correlated Electron Phases in Two Dimensions. Purdue University, 2015.

12. Beenakker, C. W. J., Theory of Coulomb-blockade oscillations in the conductance of a quantum dot. *Physical Review B* **1991,** *44* (4), 1646-1656.

13. Bergsten, T.; Claeson, T.; Delsing, P., A fast, primary Coulomb blockade thermometer. *Applied Physics Letters* **2001,** *78* (9), 1264-1266.

14. Kauppinen, J. P.; Loberg, K. T.; Manninen, A. J.; Pekola, J. P.; Voutilainen, R. A., Coulomb blockade thermometer: Tests and instrumentation. *Review of Scientific Instruments* **1998,** *69* (12), 4166-4175.

15. Maradan, D.; Casparis, L.; Liu, T. M.; Biesinger, D. E. F.; Scheller, C. P.; Zumbühl, D. M.; Zimmerman, J. D.; Gossard, A. C., GaAs Quantum Dot Thermometry Using Direct Transport and Charge Sensing. *Journal of Low Temperature Physics* **2014,** *175* (5-6), 784-798.

16. Prance, J. R.; Smith, C. G.; Griffiths, J. P.; Chorley, S. J.; Anderson, D.; Jones, G. A.; Farrer, I.; Ritchie, D. A., Electronic refrigeration of a two-dimensional electron gas. *Phys Rev Lett* **2009,** *102* (14), 146602.

17. van Wees, B. J.; van Houten, H.; Beenakker, C. W.; Williamson, J. G.; Kouwenhoven, L. P.; van der Marel, D.; Foxon, C. T., Quantized conductance of point contacts in a two-dimensional electron gas. *Phys Rev Lett* **1988,** *60* (9), 848-850.

18. Fallahi, S.; Nakamura, J. R.; Gardner, G. C.; Yannell, M. M.; Manfra, M. J., Impact of Silicon Doping on Low-Frequency Charge Noise and Conductance Drift in

GaAs/AlxGa1−xAs

Nanostructures. *Physical Review Applied* **2018,** *9* (3).

19. Ihn, T., *Semiconductor Nanostructures Quantum States and Semiconductor Transport*. Oxford University Press: 2010.

20. Foxman, E. B.; McEuen, P. L.; Meirav, U.; Wingreen, N. S.; Meir, Y.; Belk, P. A.; Belk, N. R.; Kastner, M. A.; Wind, S. J., Effects of quantum levels on transport through a Coulomb island. *Physical Review B* **1993,** *47* (15), 10020-10023.

21. Foxman, E. B.; Meirav, U.; McEuen, P. L.; Kastner, M. A.; Klein, O.; Belk, P. A.; Abusch, D. M.; Wind, S. J., Crossover from single-level to multilevel transport in artificial atoms. *Physical Review B* **1994,** *50* (19), 14193-14199.